Combining Electromagnetic and Gravitational-Wave Constraints on Neutron-Star Masses and Radii

Mohammad Al-Mamun,[1] Andrew W. Steiner,[1,2] Joonas Nättilä,[3,4] Jacob Lange,[5] Richard O'Shaughnessy,[5] Ingo Tews,[6] Stefano Gandolfi,[6] Craig Heinke,[7] and Sophia Han[8,9]

[1]*Department of Physics and Astronomy, University of Tennessee, Knoxville, Tennessee 37996, USA*
[2]*Physics Division, Oak Ridge National Laboratory, Oak Ridge, Tennessee 37831, USA*
[3]*Physics Department and Columbia Astrophysics Laboratory, Columbia University, 538 West 120th Street, New York, New York 10027, USA*
[4]*Center for Computational Astrophysics, Flatiron Institute, 162 Fifth Avenue, New York, New York 10010, USA*
[5]*Rochester Institute of Technology, 85 Lomb Memorial Drive, Rochester, New York 14623, USA*
[6]*Theoretical Division, Los Alamos National Laboratory, Los Alamos, New Mexico 87545, USA*
[7]*Department of Physics, CCIS 4-183, University of Alberta, Edmonton, Alberta T6G 2E1, Canada*
[8]*Department of Physics, University of California, Berkeley, California 94720, USA*
[9]*Department of Physics and Astronomy, Ohio University, Athens, Ohio 45701, USA*

We perform a joint Bayesian inference of neutron-star mass and radius constraints based on GW170817, observations of quiescent low-mass x-ray binaries (QLMXBs), photospheric radius expansion x-ray bursting sources, and x-ray timing observations of J0030 + 0451. With this dataset, the form of the prior distribution still has an impact on the posterior mass-radius curves and equation of state (EOS), but this impact is smaller than recently obtained when considering QLMXBs alone. We analyze the consistency of the electromagnetic data by including an "intrinsic scattering" contribution to the uncertainties, and find only a slight broadening of the posteriors. This suggests that the gravitational-wave and electromagnetic observations of neutron-star structure are providing a consistent picture of the neutron-star mass-radius curve and the EOS.

The idea that neutron stars (NSs) might be useful in determining the equation of state (EOS) of dense matter [1] precedes the discovery of the first NS in 1967 [2] by almost a decade. Until recently, the strongest observational constraints on the EOS came from NS mass measurements. These mass measurements all lay in a narrow range around 1.4 $M_\odot$ [3] until the last decade, when NSs with masses near 2.0 $M_\odot$ were discovered [4–8]. Measurements of NS radii, on the other hand, have been plagued with various systematic uncertainties [9]. The past decade has seen an increasing number of observations which constrain both the NS mass and radius with better-controlled systematic uncertainties, providing stronger EOS constraints. Quiescent low-mass x-ray binaries [10] (QLMXBs), photospheric radius expansion x-ray bursting sources [11] (PREs), and nearby isolated NSs [12,13] all have been used to provide mass and radius measurements (see, e.g., Refs. [14,15] for recent reviews). Importantly, these measurements rely on data from various different instruments and connect the radius to the actual observables using different theoretical assumptions. These in turn all yield different underlying systematics. Finally, the recent observations of gravitational waves (GWs) from binary NS mergers (GW170817 and GW190425) [16–18] by the LIGO Scientific- and Virgo Collaborations (LVCs) or x-ray observations of J0030 + 0451 by the NICER Collaboration [19,20] provide additional information on the EOS.

There are several recent works which analyze the data from GW170817 and/or GW190425 as well as NICER and its implication on the NS EOS [21–40], but very few (e.g., Refs. [31,41]) directly combine the GW data with constraints on NS radii from QLMXBs and PREs. However, these additional observational sources add valuable information. Reference [42] used QLMXB and PRE observations to *predict* the NS tidal deformability which would be inferred from GW observations. They predicted the 95% credible interval for the dimensionless tidal deformability of a 1.4 $M_\odot$ NS, $\Lambda_{M=1.4}$, was between 130 and 460. The recent analysis of GW 170817 [17] by the LVCs found the 90% credible interval $\Lambda_{M=1.4} \in [70, 580]$, to 90%, matching the prediction to within errors.

In this Letter, we present a Bayesian inference of the NS structure data, including both GW data as well as data from electromagnetic (EM) observation of QLMXBs and PREs, using less restrictive assumptions than made in previous works.

We build upon the methods described in Refs. [43–58] (see also Refs. [59,60]), reviewed in Ref. [61], and detailed

in the Supplemental Material [62] with additional references. Reference [63] first demonstrated that the choice of EOS parameterization has a significant impact on both the posterior mass-radius relation and the EOS, see also Ref. [64]. To estimate the impact of that choice, here as in Ref. [65], our prior distribution is built on two EOS parameterizations: (1) one which uses three polytropes (referred to as "3P") and (2) one which uses four line segments in the space of pressure vs energy density (referred to as "4L"). The latter parametrization has a stronger preference for strong phase transitions (regions where the pressure is nearly independent of the energy density). We use these parameterizations because both of them are physically reasonable, yet they give qualitatively different mass-radius curves. This allows us to study how the prior choice creates additional uncertainty in our results.

At each point in our EOS parameter spaces, we solve the Tolman-Oppenheimer-Volkov (TOV) equations [66,67], compute the moment of inertia as a function of the central pressure, and use the Yagi-Yunes (YY) correlation [68] (as formulated in Ref. [69]) to compute the tidal deformability as a function of central pressure. This method of computing the tidal deformability is much faster than a direct computation, and while deviations from the exact result of up to 10% are possible [70,71], the correlation is accurate to within a few percent for the typical EOS in our prior and posterior distributions. We construct the conditional probability for QLMXBs as in Ref. [65] and generalize it to include three PREs [72,73]. We also include the LIGO constraints on $\tilde{\Lambda}$ from GW170817, using the SEOBNRv4T model for a binary NS inspiral assuming low compact object spins [74]. GW observations are incorporated by tabulating and interpolating a marginal likelihood versus the masses for each object and the combined tidal deformability. Marginalization is performed via RIFT [75] over all extrinsic parameters and our fiducial low-spin prior assumptions. Finally, we also include mass and radius constraints on J0030 + 0451 from the NICER instrument [19,20]. We reject all EOSs which are acausal or imply a maximum NS mass less than 2 $M_\odot$. The mass cutoff does have a small uncertainty, but this uncertainty does not qualitatively impact our results. Also, we could have chosen to replace one of the high-density EOS parameters with M_{max}, but since neither the high-density part of the EOS nor the maximum mass is well known, this prior choice is not necessarily better (or worse) than ours.

While it is often helpful to directly model systematic uncertainties, as was partially done in earlier works [65,72,73], these estimations require detailed models for the uncertainties which may not be perfect. Systematic uncertainties may result in intrinsic scattering (IS) which we model by convolving the probability distribution for each star with a Gaussian kernel. This addition of an extra uncertainty to the observations allows us to *quantify* the possible level of systematic bias present in each measurement: the value of each IS parameter is expected to increase

until the full dataset used in the inference is self-consistent. We emphasize that there is no reason to believe that a Gaussian is necessarily the *correct* distribution for additional unknown systematics, but we believe it is a reasonable first guess. Our approach is based on the intrinsic scattering parameter from Ref. [73] which was applied to the x-ray spectrum rather than the mass and radius constraints. The details of this procedure and the Markov Chain Monte Carlo (MCMC) method are given in the Supplemental Material [62].

We argue that neither of the two EOS parameterizations are more or less motivated by quantum chromodynamics (QCD), and thus we assign them equal prior probability. We present the posteriors for these two EOS parameterizations, 3P and 4L, separately to make the impact of a different EOS parameterization clear. We also present four different datasets: (i) GW170817 only (GW), (ii) GW170817 + QLMXBs + PREs (GW, QLMXB, PRE), (iii) GW170817 + QLMXBs + PREs + NICER (all), and (iv) GW170817 + QLMXBs + PREs + NICER with an additional intrinsic scattering parameter added to each of the QLMXBs, PREs, and NICER (all + IS). We thus performed eight different sets of simulations.

Posteriors for the radius of a 1.4 solar mass NS, $R_{1.4}$, are summarized in Fig. 1. As might be expected, the limits for the GW data alone [(a) and (b)] are the least constraining. The 95% credible intervals are 11.3–13.9 km (3P) and 10.7–13.1 km (4L). Choosing a line segment-based EOS prior decreases the lower (upper) radius limit by 0.5 (1) km. The next four bar plots in the figure [(c)–(f)] show that the range shrinks significantly when adding the EM observations without IS. Because the GW posteriors are weighted towards larger radii, including the EM observations alone
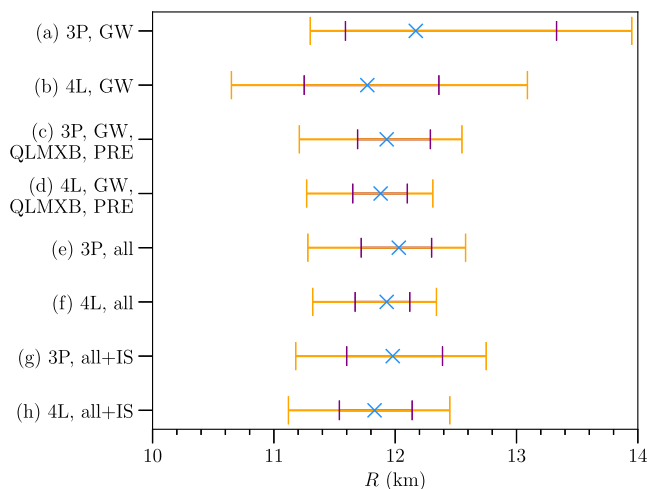

FIG. 1. Radius measured for a 1.4 $M_\odot$ NS in different models and with different data sets. Ranges labeled (a), (c), (e) and, (g) refer to radii obtained with the 3P EOS. Ranges labeled (b), (d), (f) and, (h) were obtained with 4L EOS. Blue crosses indicate the maximum a posteriori estimate ("MAP") points, while the purple and orange bars represent the 68% and 95% credible intervals.
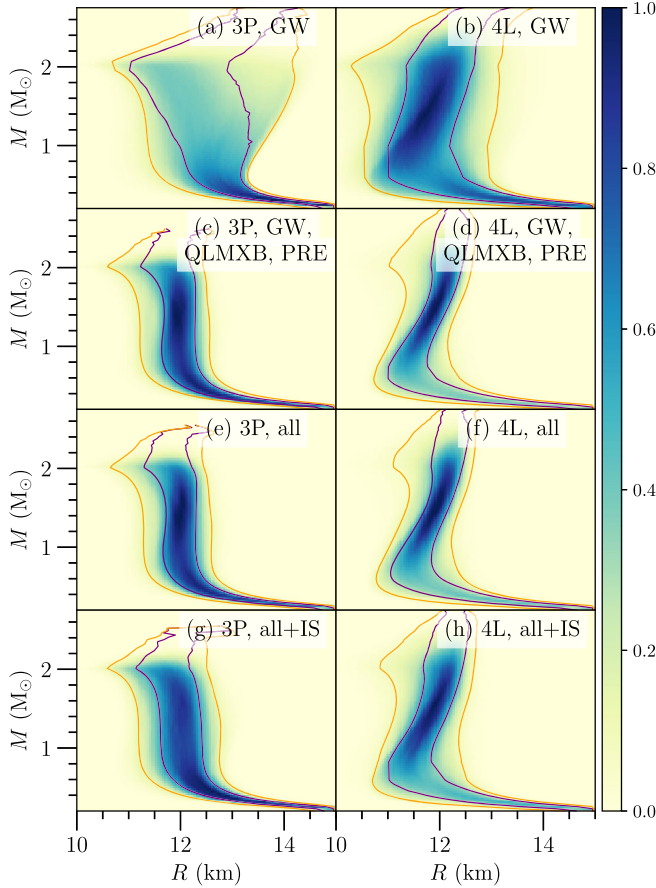
FIG. 2. Posterior distributions for the NS radius as a function of the gravitational mass. Left panels [(a), (c), (e), (g)] are constructed with the 3P EOS and right panels [(b), (d), (f), (h)] with the 4L EOS. Different rows refer to different data selections.
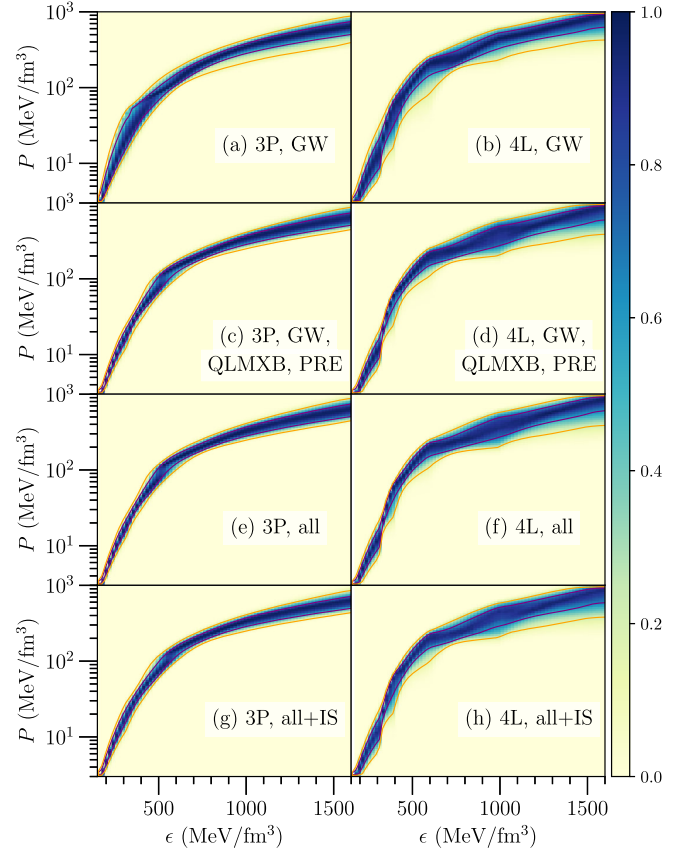

FIG. 3. Posterior distributions for the pressure as a function of the energy density. Left panels [(a), (c), (e), (g)] are constructed with the 3P EOS and right panels [(b), (d), (f), (h)] with the 4L EOS. Different rows refer to different data selections.

would shift the results in panels (e) and (f) very slightly towards lower radii. In addition, once the EM observations are added, these constraints are less sensitive to the EOS prior than the QLMXB observations alone [65]. Including the IS contribution [(g) and (h)] slightly broadens the constraints coming from the EM data.

Figure 2 shows the posterior distributions for the NS radius as a function of the gravitational mass. The shape of the mass-radius curve is more sensitive to the EOS prior than the radius of a 1.4 solar mass NS alone. The 4L EOS prior, because of the potential for phase transitions to modify the EOS at low densities, produces smaller radii for low-mass stars and larger radii for high-mass stars. This distinction may be particularly important in light of a possible 2.6 $M_\odot$ NS in GW190814 [76–78].

Figure 3 shows the posteriors for the pressure as a function of the energy density. The combination of the EM and GW data strongly constrains the pressure until about 400–500 MeV/fm³. In order to more easily compare the pressures between different models or datasets, Fig. 4 shows an alternate version where, for each energy density, all eight panels are rescaled and shifted by the same linear

transformation which ensures that the 95% credible intervals for panel (a) lie exactly at 0 and 1. Thus, for panels (b) through (h), the orange dashed curves show the change in pressure of different models relative to that in panel (a). For reference, the energy density at nuclear saturation is $\epsilon_0 \approx 150$ MeV/fm³. The red dot-dashed curves show the probability that the central energy density of the maximum mass NS is smaller than the energy density from the x axis. Most EOSs suggested by the data imply the central energy density is between about 900 and 1200 MeV/fm³. In the 3P model, the EM data suggest a smaller pressure for small energy densities and almost unchanged at higher densities. In the 4L model, the effect is more dramatic: a smaller pressure at low densities is compensated for by an increase in the pressure at higher densities. For $\epsilon > 1200$ MeV/fm³, it is unlikely the data are strongly constraining the EOS, i.e., the EOS is strongly impacted by the prior distribution.

We compare our results to several other previous works in Table I. Our results on $R_{1.4}$ with the GW data alone are consistent with previous works which include only limited information from NS radius constraints [21,23,27–30,39]. The variation in these results across the various references is consistent with our finding that these posterior
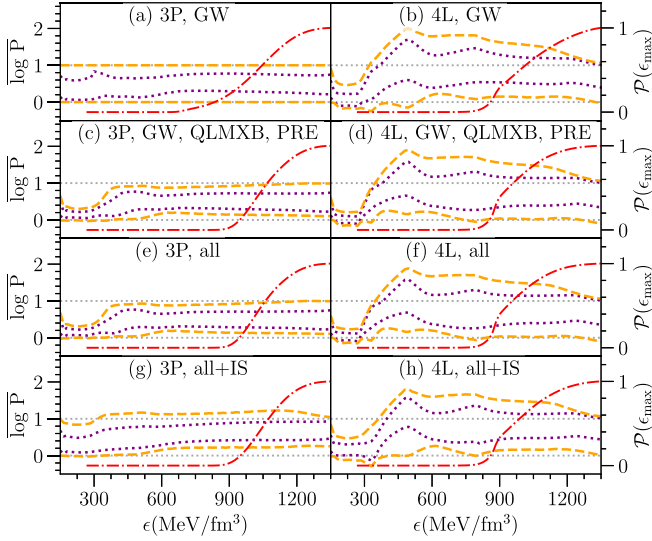
FIG. 4. The 68% (purple dotted line) and 95% (orange dashed line) credible intervals for the pressure as a function of the energy density. All intervals are modified with the same linear transformation to ensure that the upper and lower 95% intervals in panel (a) are always at 0 and 1. The right-hand y axis (red dot-dashed line) shows the posterior probability that the central energy density is smaller than the value on the x axis. The different panels refer to different models and different data selections as in Figs. 2 and 3.

distributions depend on the EOS prior distribution (as well as on the other details of the analysis).

Other works find, as we do, that the radius constraints are tighter when the EM data are included. Our results which include IS suggest (but do not definitively prove) that this result is not due to systematic uncertainties which are artificially constraining NS radii.

Gravitational-wave observations have suggested other possible more indirect constraints on the EOS, and we summarize the impact of some of these constraints have on the radius of a 1.4 $M_\odot$ NS in Table II by applying them to our "all + IS" posteriors. References [29,79] found that GW170817 implied a lower limit on $\tilde\Lambda > 300$, because EOSs with smaller values of $\tilde\Lambda$ do not create a sufficiently massive accretion disk to the observed kilonova. This constraint may be optimistic (e.g., see Ref. [80]) (and see also a different perspective in Ref. [81]), but it has a relatively low impact. It increases the lower limit on the 95% credible interval for $R_{1.4}$ by about 0.2 km. Reference [82] found that $M_{max} \leq 2.17 M_\odot$ was required to ensure that no short-lived hypermassive NS (which was not observed) was present in GW170817. We find that this constraint has only a weak impact on our posterior distributions. The maximum mass is weakly correlated by the radius of a 1.4 solar mass NS, as shown in the Supplemental Material [62], so when we decrease the typical maximum mass we also slightly decrease the typical radius. GW190814 implied the merger of a 2.6 $M_\odot$ object

TABLE I. A comparison of our posterior distributions for the radius of a 1.4 $M_\odot$ NS in comparison to other results obtained in the literature.

Reference	$R_{1.4}$	Credible interval	Source
[17]	[10.5, 13.3]	90%	GW
[21]	[9.9, 13.6]	90%	GW
[22]	< 13.6	90%	GW
[23]	[9.4, 12.8]	90%	GW
[27]	[9.8, 13.2] [a]	90%	GW
[36]	[10.36, 12.78]	90%	GW
Model "a"	[11.30, 13.95]	95%	GW
Model "b"	[10.65, 13.09]	95%	GW
[28]	[8.9, 13.2]	90%	GW, merger remnant
[29]	[11.4, 13.2]	90%	GW, merger remnant
[30]	[10.4, 11.9]	90%	GW, merger remnant
[31]	[11.98, 12.76]	90%	GW, QLMXB
[32]	[10.5, 11.8]	90%	GW, QLMXB
[33]	[10.94, 12.72]	90%	GWs [b], NICER
[34,35]	[10.85, 13.41]	90%	GWs, NICER
[36]	[11.91, 13.25]	90%	GW, NICER
[37]	[11.3, 13.3]	90%	GW, NICER
[41]	[12, 13]	90%	GWs, NICER
[41]	[10.0, 11.5]	90%	GWs, QLMXB, PRE
Model "c"	[11.21, 12.55]	95%	GW, QLMXB, PRE
Model "e"	[11.28, 12.58]	95%	GW, QLMXB, PRE, NICER

[a]Radius measurement for the primary NS of the merger event.
[b]GWs refer to the joint analysis of GW170817 and GW190425.

with a more massive black hole. Our MCMC simulation for the 3P model generated no configurations with maximum masses this large. This does not necessarily mean that 3P parameter sets with large maximum masses do not exist, but they do appear highly improbable. In the 4L model, increasing M_{max} to 2.6 $M_\odot$ increases the 95% lower limit for the radius by 0.5 km. For example, in Table II, changing the M_{max} value in 4L models increased the R lower limit of 95% credible interval from 10.98 km to 11.47 km for a 1.4 $M_\odot$ NS. An alternate explanation for GW190814 is that rotation is supporting a larger maximum mass [83,84]. Finally, correlations from Refs. [28,85–87] are tested in the Supplemental Material [62].

TABLE II. The 68% and 95% credible intervals for the radius of a 1.4 $M_\odot$ NS in km with applied constraints on intrinsic scattering models.

Model and constraints	-2σ	-1σ	$+1\sigma$	$+2\sigma$
3P, all + IS	11.18	11.6	12.39	12.75
4L, all + IS	11.12	11.54	12.14	12.45
3P, all + IS ($\tilde\Lambda > 300$)	11.33	11.63	12.37	12.71
4L, all + IS ($\tilde\Lambda > 300$)	11.28	11.56	12.12	12.40
3P, all + IS ($M_{max} < 2.17 M_\odot$)	11.15	11.54	12.31	12.72
4L, all + IS ($M_{max} < 2.17 M_\odot$)	10.98	11.43	12.13	12.46
4L, all + IS ($M_{max} > 2.6 M_\odot$)	11.47	11.76	12.19	12.42

[1] A. G. Cameron, Astrophys. J. **130**, 884 (1959).
[2] A. Hewish, S. J. Bell, J. D. H. Pilkington, P. F. Scott, and R. A. Collins, Nature (London) **217**, 709 (1968).
[3] S. E. Thorsett and D. Chakrabarty, Astrophys. J. **512**, 288 (1999).
[4] O. Barziv, L. Kaper, M. H. Van Kerkwijk, J. H. Telting, and J. Van Paradijs, Astron. Astrophys. **377**, 925 (2001).
[5] P. B. Demorest, T. Pennucci, S. M. Ransom, M. S. E. Roberts, and J. W. T. Hessels, Nature (London) **467**, 1081 (2010).
[6] M. H. van Kerkwijk, R. P. Breton, and S. R. Kulkarni, Astrophys. J. **728**, 95 (2011).
[7] J. Antoniadis, P. C. C. Freire, N. Wex, T. M. Tauris, R. S. Lynch, M. H. van Kerkwijk, M. Kramer, C. Bassa, V. S. Dhillon, T. Driebe et al., Science **340**, 1233232 (2013).
[8] H. T. Cromartie, E. Fonseca, S. M. Ransom, P. B. Demorest, Z. Arzoumanian, H. Blumer, P. R. Brook, M. E. DeCesar, T. Dolch, J. A. Ellis et al., Nat. Astron. **4**, 72 (2020).
[9] J. M. Lattimer and M. Prakash, Phys. Rep. **442**, 109 (2007); the Hans Bethe Centennial Volume 1906–2006.
[10] C. O. Heinke, G. B. Rybicki, R. Narayan, and J. E. Grindlay, Astrophys. J. **644**, 1090 (2006).
[11] F. Özel, T. Güver, and D. Psaltis, Astrophys. J. **693**, 1775 (2009).
[12] J. A. Pons, F. M. Walter, J. M. Lattimer, M. Prakash, R. Neuhauser, and P.-h. An, Astrophys. J. **564**, 981 (2002).
[13] W. C. G. Ho and C. O. Heinke, Nature (London) **462**, 71 (2009).
[14] J. M. Lattimer, Annu. Rev. Nucl. Part. Sci. **62**, 485 (2012).
[15] F. Ozel and P. Freire, Annu. Rev. Astron. Astrophys. **54**, 401 (2016).
[16] LIGO Scientific and Virgo Collaborations, Phys. Rev. Lett. **119**, 161101 (2017).
[17] LIGO Scientific and Virgo Collaborations, Phys. Rev. Lett. **121**, 161101 (2018).

[18] B. Abbott et al. (LIGO Scientific and Virgo Collaborations), Astrophys. J. Lett. **892**, L3 (2020).
[19] T. E. Riley, A. L. Watts, S. Bogdanov, P. S. Ray, R. M. Ludlam, S. Guillot, Z. Arzoumanian, C. L. Baker, A. V. Bilous, D. Chakrabarty et al., Astrophys. J. **887**, L21 (2019).
[20] M. C. Miller et al., Astrophys. J. **887**, L24 (2019).
[21] E. Annala, T. Gorda, A. Kurkela, and A. Vuorinen, Phys. Rev. Lett. **120**, 172703 (2018).
[22] F. J. Fattoyev, J. Piekarewicz, and C. J. Horowitz, Phys. Rev. Lett. **120**, 172702 (2018).
[23] B. Kumar and P. Landry, Phys. Rev. D **99**, 123026 (2019).
[24] M. W. Coughlin et al., Mon. Not. R. Astron. Soc. **480**, 3871 (2018).
[25] M. W. Coughlin, T. Dietrich, B. Margalit, and B. D. Metzger, Mon. Not. R. Astron. Soc. **489**, L91 (2019).
[26] I. Tews, J. Margueron, and S. Reddy, Phys. Rev. C **98**, 045804 (2018).
[27] C. A. Raithel, Eur. Phys. J. A **55**, 80 (2019).
[28] S. De, D. Finstad, J. M. Lattimer, D. A. Brown, E. Berger, and C. M. Biwer, Phys. Rev. Lett. **121**, 091102 (2018).
[29] D. Radice and L. Dai, Eur. Phys. J. A **55**, 50 (2019).
[30] C. D. Capano, I. Tews, S. M. Brown, B. Margalit, S. De, S. Kumar, D. A. Brown, B. Krishnan, and S. Reddy, Nat. Astron., **4**, 625 (2020).
[31] N. B. d'Etivaux, S. Guillot, J. Margueron, N. Webb, M. Catelan, and A. Reisenegger, Astrophys. J. **887**, 48 (2019).
[32] J.-L. Jiang, S.-P. Tang, D.-S. Shao, M.-Z. Han, Y.-J. Li, Y.-Z. Wang, Z.-P. Jin, Y.-Z. Fan, and D.-M. Wei, Astrophys. J. **885**, 39 (2019).
[33] T. Dietrich, M. W. Coughlin, P. T. Pang, M. Bulla, J. Heinzel, L. Issa, I. Tews, and S. Antier, Science **370**, 1450 (2020).
[34] P. Landry and R. Essick, Phys. Rev. D **99**, 084049 (2019).
[35] P. Landry, R. Essick, and K. Chatziioannou, Phys. Rev. D **101**, 123007 (2020).
[36] R. Essick, I. Tews, P. Landry, S. Reddy, and D. E. Holz, Phys. Rev. C **102**, 055803 (2020).
[37] J.-L. Jiang, S.-P. Tang, Y.-Z. Wang, Y.-Z. Fan, and D.-M. Wei, Astrophys. J. **892**, 55 (2020).
[38] J. M. Lattimer, Universe **5**, 159 (2019).
[39] A. Ayriyan, D. Alvarez-Castillo, D. Blaschke, and H. Grigorian, Universe **5**, 61 (2019).
[40] G. Raaijmakers et al., Astrophys. J. Lett. **893**, L21 (2020).
[41] C. Raithel, F. Ozel, and D. Psaltis, arXiv:2004.00656.
[42] A. W. Steiner, S. Gandolfi, F. J. Fattoyev, and W. G. Newton, Phys. Rev. C **91**, 015804 (2015).
[43] J. B. Hartle, Astrophys. Suppl. Ser. **24**, 385 (1973).
[44] K. E. Schmidt and S. Fantoni, Phys. Lett. B **446**, 99 (1999).
[45] J. Goodman and J. Weare, Commun. Appl. Math. Comput. Sci. **5**, 65 (2010).
[46] A. W. Steiner, J. M. Lattimer, and E. F. Brown, Astrophys. J. **722**, 33 (2010).
[47] A. W. Steiner and S. Gandolfi, Phys. Rev. Lett. **108**, 081102 (2012).
[48] S. Gandolfi, J. Carlson, and S. Reddy, Phys. Rev. C **85**, 032801(R) (2012).
[49] A. Gezerlis, I. Tews, E. Epelbaum, M. Freunek, S. Gandolfi, K. Hebeler, A. Nogga, and A. Schwenk, Phys. Rev. C **90**, 054323 (2014).

[50] J. J. E. Kajava, J. Nättilä, O.-M. Latvala, M. Pursiainen, J. Poutanen, V. F. Suleimanov, M. G. Revnivtsev, E. Kuulkers, and D. K. Galloway, Mon. Not. R. Astron. Soc. **445**, 4218 (2014).

[51] M. Kortelainen, J. McDonnell, W. Nazarewicz, E. Olsen, P.-G. Reinhard, J. Sarich, N. Schunck, S. M. Wild, D. Davesne, J. Erler *et al.*, Phys. Rev. C **89**, 054314 (2014).

[52] J. D. McDonnell, N. Schunck, D. Higdon, J. Sarich, S. M. Wild, and W. Nazarewicz, Phys. Rev. Lett. **114**, 122501 (2015).

[53] J. E. Lynn, I. Tews, J. Carlson, S. Gandolfi, A. Gezerlis, K. E. Schmidt, and A. Schwenk, Phys. Rev. Lett. **116**, 062501 (2016).

[54] I. Tews, S. Gandolfi, A. Gezerlis, and A. Schwenk, Phys. Rev. C **93**, 024305 (2016).

[55] A. W. Steiner, arXiv:1802.05339.

[56] A. W. Shaw, C. O. Heinke, A. W. Steiner, S. Campana, H. N. Cohn, W. C. G. Ho, P. M. Lugger, and M. Servillat, Mon. Not. R. Astron. Soc. **476**, 4713 (2018).

[57] S. Gandolfi, J. Lippuner, A. W. Steiner, I. Tews, X. Du, and M. Al-Mamun, J. Phys. G **46**, 103001 (2019).

[58] X. Du, A. W. Steiner, and J. W. Holt, Phys. Rev. C **99**, 025803 (2019).

[59] J. S. Read, B. D. Lackey, B. J. Owen, and J. L. Friedman, Phys. Rev. D **79**, 124032 (2009).

[60] M. F. Carney, L. E. Wade, and B. S. Irwin, Phys. Rev. D **98**, 063004 (2018).

[61] J. M. Lattimer and A. W. Steiner, Eur. Phys. J. A **50**, 40 (2014).

[62] See Supplemental Material at http://link.aps.org/supplemental/10.1103/PhysRevLett.126.061101 for more detail on the neutron star models, more computational details, and additional results on tidal deformability and radius correlations.

[63] A. W. Steiner, J. M. Lattimer, and E. F. Brown, Astrophys. J. Lett. **765**, L5 (2013).

[64] S. Greif, G. Raaijmakers, K. Hebeler, A. Schwenk, and A. Watts, Mon. Not. R. Astron. Soc. **485**, 5363 (2019).

[65] A. W. Steiner, C. O. Heinke, S. Bogdanov, C. Li, W. C. G. Ho, A. Bahramian, and S. Han, Mon. Not. R. Astron. Soc. **476**, 421 (2018).

[66] R. C. Tolman, Phys. Rev. **55**, 364 (1939).

[67] J. Oppenheimer and G. Volkoff, Phys. Rev. **55**, 374 (1939).

[68] K. Yagi and N. Yunes, Science **341**, 365 (2013).

[69] A. W. Steiner, J. M. Lattimer, and E. F. Brown, Eur. Phys. J. A **52**, 18 (2016).

[70] S. Han and A. W. Steiner, Phys. Rev. D **99**, 083014 (2019).

[71] Z. Carson, K. Chatziioannou, C.-J. Haster, K. Yagi, and N. Yunes, Phys. Rev. D **99**, 083016 (2019).

[72] J. Nättilä, A. W. Steiner, J. J. E. Kajava, V. F. Suleimanov, and J. Poutanen, Astron. Astrophys. **591**, A25 (2016).

[73] J. Nättilä, M. C. Miller, A. W. Steiner, J. J. E. Kajava, V. F. Suleimanov, and J. Poutanen, Astron. Astrophys. **608**, A31 (2017).

[74] LIGO Scientific and Virgo Collaborations, Phys. Rev. X **9**, 011001 (2019).

[75] J. Lange, R. O'Shaughnessy, and M. Rizzo, arXiv:1805.10457.

[76] R. Abbott *et al.* (LIGO Scientific and Virgo Collaborations), Astrophys. J. Lett. **896**, L44 (2020).

[77] R. Essick and P. Landry, Astrophys. J. **904**, 80 (2020).

[78] I. Tews, P. T. Pang, T. Dietrich, M. W. Coughlin, S. Antier, M. Bulla, J. Heinzel, and L. Issa, arXiv:2007.06057.

[79] D. Radice, A. Perego, F. Zappa, and S. Bernuzzi, Astrophys. J. Lett. **852**, L29 (2018).

[80] A. Bauswein and N. Stergioulas, Mon. Not. R. Astron. Soc. **471**, 4956 (2017).

[81] K. Kiuchi, K. Kyutoku, M. Shibata, and K. Taniguchi, Astrophys. J. Lett. **876**, L31 (2019).

[82] M. Ruiz, S. L. Shapiro, and A. Tsokaros, Phys. Rev. D **97**, 021501(R) (2018).

[83] N.-B. Zhang and B.-A. Li, Astrophys. J. **902**, 38 (2020).

[84] V. Dexheimer, R. Gomes, T. Klähn, S. Han, and M. Salinas, arXiv:2007.08493.

[85] J. M. Lattimer and M. Prakash, Astrophys. J. **550**, 426 (2001).

[86] K. Yagi and N. Yunes, Classical Quantum Gravity **34**, 015006 (2017).

[87] A. Maselli, V. Cardoso, V. Ferrari, L. Gualtieri, and P. Pani, Phys. Rev. D **88**, 023007 (2013).

[88] A. W. Steiner, bamr: Bayesian analysis of mass and radius observations (2014), Astrophysics Source Code Library, record ascl:1408.020.

[89] A. W. Steiner, O2scl: Object-oriented scientific computing library (2014), Astrophysics Source Code Library, record ascl:1408.019.

[90] F. Frigo and S. G. Johnson, Fftw: Fastest fourier transform in the west (2012), FFTW: Fastest Fourier Transform in the West, record ascl:1201.015.